FT-Infrared Spectroscopic Studies of the Iron Ligand CO Stretch Mode of iNOS Oxygenase Domain: Effect of Arginine and Tetrahydrobiopterin†

Christiane Jung*,‡ Dennis J. Stuehr,§ and Dipak K. Ghosh*,||

Max-Delbrück-Center for Molecular Medicine, Robert-Rössle-Strasse 10, D-13092 Berlin, Germany, Department of Immunology, The Cleveland Clinic, Cleveland, Ohio 44195, and Department of Medicine, Duke University and VA Medical Center, Durham, North Carolina 27713

Received February 17, 2000; Revised Manuscript Received May 22, 2000

ABSTRACT: The iron ligand CO stretch vibration mode of the inducible nitric oxide synthase oxygenase domain (iNOSox) has been studied from 20 to 298 K. iNOSox in the absence of arginine reveals a temperature-dependent equilibrium of two major conformational substates with CO stretch bands centered at about 1945 and 1954 cm^{-1}. This behavior is not qualitatively changed when tetrahydrobiopterin (H_4B) is bound. Arginine binding changes significantly the spectrum by formation of a sharp CO stretch mode band at about 1905 cm^{-1} and indicates the formation of a hydrogen bond to the CO ligand. For temperatures lower than 250 K, the stretch vibration frequency decreases almost linearly with decreasing temperature and indicates that the coupling between the CO ligand and the arginine/protein in the active site via the hydrogen bond is very strong. Flashphotolysis of the CO ligand carried out at 25 K revealed the CO stretch mode of the photodissociated CO ligand trapped in the heme pocket. There is a negative linear relation between the stretch vibration frequencies of the photodissociated and the iron-bound CO indicating that the photodissociated ligand stays near the heme.

Nitric oxide (NO)[1] synthase occurs in a wide variety of cell types and tissues including the vascular endothelium, platelets, macrophages, and neuronal cells (*1*, *2*). The research in nitric oxide has attracted scientists from all disciplines in the recent years because of its versatile role in physiology and pathobiology. NO is involved in the regulation of various physiological processes including blood pressure, neurotransmission, insulin release, memory storage, and immune response. However, in reaction with reactive oxygen species, NO produces cytotoxic agents that cause cell death and toxicity (*3*). The biogenesis of nitric oxide is catalyzed by NO synthases (NOSs) that form L-citrulline and NO through a stepwise NADPH and O_2-dependent oxidation of L-arginine (*4*). NO synthases form a family of three distinct genetically encoded isoforms: neuronal (nNOS), endothelial (eNOS), and cytokine inducible (iNOS) synthase (*4*−*7*). In the active form, all three enzymes are homodimeric proteins whose subunits are composed of an N-terminal oxygenase domain that binds iron protoporphyrin IX (heme), L-arginine, and tetrahydrobiopterin (H_4B) and a C-terminal reductase domain that binds FMN, FAD, and NADPH with an intervening calmodulin binding sequence between the two domains (*8*−*11*). The crystal structures of the oxygenase domain of mouse iNOS (*12*−*14*), eNOS (*15*), and human eNOS and iNOS (*16*, *17*) in either tetrahydrobiopterin bound or with arginine have recently been determined. Examination of these structures revealed that the core structure of the oxygenase domain is formed by one continuous fold made up of several winged β-sheets, the unique structural feature present in all NOS isoforms. This structure distinguishes the NOS enzyme from that of the cytochrome P450 superfamily whose folds are mainly composed of α-helix and β-sheets. In addition, dimerization may bring loops and helical elements from both N- and C-terminal ends of the core oxygenase domain into a central region that forms an extensive dimer interface, H_4B binding site and substrate channel (*13*, *14*). Residues that participate in L-arginine and H_4B binding and the molecular interactions involved are well-documented and clearly defined in those structures. In contrast to this structural information, the enzyme reaction mechanism is not completely understood. The proposed mechanism of NO synthesis suggests similarities to cytochrome P450 regarding heme-based, stepwise activation of

†This work was supported by grants from the Deutsche Forschungsgemeinschaft (Grant Sk35/3-1,2) and the National Institutes of Health (CA53914, D.J.S.).

* To whom correspondence should be addressed. PD Dr. Christiane Jung, Max-Delbrück-Center for Molecular Medicine, Protein Dynamics, Robert-Rössle-Strasse 10, D-13092 Berlin, Germany. Telephone: (49)-30−94063370. Fax: (49)-30-94063329. E-mail: cjung@mdc-berlin.de, and Dr. Dipak K. Ghosh, Department of Medicine, Duke University and VA Medical Center, 508 Fulton Street, Durham, NC 27705, USA. Telephone: (919) 286-0411 ext 5249. Fax: (919) 286-6891. E-mail: dgx@acpub.duke.edu.

‡ Max-Delbrück-Center for Molecular Medicine.

§ The Cleveland Clinic.

|| Duke University and VA Medical Center.

[1] Abbreviations: NO, nitric oxide; NOS, nitric oxide synthase; iNOS, inducible NOS; eNOS, endothelial NOS; nNOS, neuronal NOS; iNOSox, inducible nitric oxide synthase oxygen domain; arg, L-arginine; DTT, dithiothreitol; EPPS, *N*-(2-hydroxyethyl)piperazine-*N*′-(3-propane sulfonic acid); H_4B, (6R)-5,6,7,8-tetrahydro-L-biopterin; PTFE, polytetrafluoroethylen; KP, potassium phosphate buffer; $P450_{cam}$, cytochrome $P450_{cam}$ from *Pseudomonas putida* (CYP101); P420, denatured form of a thiolate heme protein showing the electronic absorption band (Soret) in the carbon monoxide complex at 420 nm; FTIR, Fourier transform infrared spectroscopy; FMN, flavin mononucleotide; FAD, flavin adenine dinucleotide; NADPH, nicotinamide adenine dinucleotide phosphate; Mb, myoglobin.

10.1021/bi0003792 CCC: $19.00
Published on Web 07/28/2000

O_2 (*4*, *18*). A detailed understanding of the reaction mechanism thus requires crystal structure data of the dioxygen complex of NOS oxygenase domain which has yet to be determined. However, the formation of the dioxygen complex of NO synthase has recently been demonstrated by various groups using rapid scanning stopped-flow, rapid mixing and low-temperature spectroscopy (*19*−*22*). Interestingly, all these studies have reported variable stability and differences in the characteristic absorption spectra. Therefore, further studies are needed to understand the mechanistic implications of the Fe^{2+}-O_2 complex with respect to arginine binding and product formation. The crystal structure data of the NOS distal heme pocket reveals that it lacks the obvious proton delivery system (*13*) that is present in cytochromes P450 to assist the O−O bond cleavage (*23*, *24*). This led to the proposition that in the absence of such a proton donor system in the NOS heme distal pocket, L-arginine may act as a proton donor to assist the oxygen activation by formation of a hydrogen bond with the ferrous dioxygen complex and thus help catalyze its own hydroxylation. This idea has already been suggested by Crane et al. (*13*).

Fourier transform infrared spectroscopy (FTIR) is an adequate method for analyzing the distal side structure using the iron ligand stretch mode as a spectroscopic probe. Unfortunately, the dioxygen complex is difficult to study by infrared spectroscopy because of its low stability. In contrast, the CO complex is stable, its CO stretch vibration appears in a free spectral window and overlapping signals from other vibrating groups are not observed. FTIR studies on many heme proteins have demonstrated that the CO stretch mode is very sensitive to structural changes on the heme distal side (*25*).

In the present paper, we report results of the first FTIR spectroscopic study of the carbon monoxide complex of iNOS oxygenase domain and of the effect of tetrahydrobiopterin and arginine binding on the CO ligand stretch mode. We studied the temperature dependence of the CO stretch mode (20−298 K) and the infrared spectrum of the photodissociated CO ligand at 25 K. This gave detailed insights into the subtle conformational behavior of iNOS as it has been demontrated for cytochrome P450 (*26*−*29*). The FT infrared spectroscopic study on iNOS, presented in this paper, suggests that arginine binding induces a hydrogen bond to the heme iron bound CO ligand that would be in line with the proposed mechanism of substrate-assisted proton donation for oxygen activation.

MATERIALS AND METHODS

Protein and Sample Preparation. Inducible nitric oxide synthase oxygenase domain (iNOSox) from mouse was produced in *Escherichia coli* as a C-terminally His6-tagged protein using the expression vector pCWori and purified as previously described (*30*). The protein was dialyzed at 4 °C against 40 mM EPPS buffer, pH 7.6, containing 5% (v/v) glycerol, and 1 mM DTT in the presence or in the absence of 4 mM H_4B. EPPS and DTT were purchased from SIGMA (St. Louis, MO). Glycerol (99.5%) and tetrahydrobiopterin were from Aldrich (Steinheim, Germany) and ICN Pharmaceuticals, Inc. (Costa Mesa, CA), respectively. All reagents have been used without further purification.

The samples for the infrared studies on H_4B-free iNOSox were concentrated to approximately 2 mM using Microcon-30 concentrators. A total of 20 μL of the concentrated protein was mixed with 30 mg of glycerol (99.5%) and 0.5 μL of 500 mM DTT and equilibrated for 8 h at 4 °C. The final buffer concentrations are 17.8 mM EPPS, pH 7.6, 5.5 mM DTT, and 57.7% (v/v) glycerol. To make the arginine complex, 1.1 μL of a 500 mM aqueous arginine solution was added to 25 μL of the arginine-free protein in the EPPS buffer−glycerol−DTT solution yielding a final arginine concentration of 21 mM. iNOSox in the absence of H_4B and arginine was also transferred into 100 mM potassium phosphate buffer, pH 7.07, by repeated concentration and dilution steps in a Microcon-30 concentrator. A total of 25 μL of the concentrated protein (1.3 mM) was mixed with 25 μL glycerol (99.5%). For the arginine complex, 1 μL of the aqueous arginine solution (500 mM) was added to 23 μL of the iNOSox sample to get a final arginine concentration of 20.8 mM. The final buffer concentration in both samples was 50 mM potassium phosphate, pH 7.07, and 50% (v/v) glycerol. In a separate solution of the same buffer composition, the pH value was checked when adding the arginine stock solution, which has a pH of 5.63. No change of the pH value of the buffer was observed. The arginine-bound iNOS sample was also studied in deuterated potassium phosphate buffer with the same composition as mentioned above. H_2O/D_2O exchange was made by repeated freeze-drying of a stock phosphate buffer of pH 7 and diluting with D_2O to achieve 100 mM final concentration. Deuterated glycerol (-d_3) was from Aldrich (Steinheim, Germany). Arginine was dissolved in D_2O.

The samples in the presence of tetrahydrobiopterin (H_4B) were obtained by concentrating the iNOSox stock solution (276 μM protein, 40 mM EPPS, pH 7.6, 5% (v/v) glycerol, and 1 mM DTT) to about 0.92 mM. Twenty microliters of this concentrated protein was mixed with 30 mg of glycerol (99.5%), 0.5 μL of aqueous DTT (500 mM), and 0.5 μL of aqueous H_4B (100 mM), which gave final concentrations of 17.8 mM EPPS, 1.1 mM H_4B, 5.5 mM DTT, and 57.7% (v/v) glycerol. To make the arginine complex of iNOSox in the presence of H_4B, 20 μL of concentrated iNOSox (0.92 mM) was mixed with 31 mg of glycerol (99.5%), 0.5 μL of H_4B (100 mM), 0.5 μL of DTT (500 mM), and 2 μL of arginine (500 mM) to obtain final concentrations of 17.8 mM EPPS, 1.14 mM H_4B, 5.94 mM DTT, 22 mM arginine, and 57.7% (v/v) glycerol. All samples were kept at 4 °C for 8 h to equilibrate the protein in the glycerol-containing solution.

The CO complex preparation for the infrared studies followed the procedures for cytochrome P450 published in previous papers (*26*, *28*, *29*, *31*). A total of 500 μL of H_2O was purged with nitrogen for at least 25 min to remove oxygen. Then, 90 mg of sodium dithionite was dissolved under oxygen-free conditions. CO gas was passed under controlled flow conditions over the surface of 40 μL of the protein solutions for 2 min. Three microliters of the dithionite solution was then added, and CO was passed over the solution surface for an additional 2 min.

Infrared Studies. A total of 10 μL of the iNOSox−CO solution was placed between CaF_2 windows separated by a 100-μm PTFE spacer in a homemade demountable infrared cell. The electronic absorption spectrum of the CO complex was measured directly in the infrared cell on the Shimadzu PC2101 spectrophotometer before mounting the cell on the

cold finger of the cryopump of the closed-cycle helium cryosystem CTI model 22C (Cryophysics). The temperature was controlled by the Lake Shore Cryogenics temperature controller (model DRC-91CA). The temperature was measured directly at the infrared cell holder near the sample using a separate silicon temperature sensor. After the cell was mounted on the cold finger, the sample was cooled to 20 K within 2 h. Spectra were taken at temperature intervals of 20 K below 160 K and at 10 K above 160 K in a warming-up mode. The sample was allowed to equilibrate at each temperature for 15 min before scanning the spectrum. The temperature was stable within 0.5 K during the measurements.

The infrared spectra were recorded on the BRUKER IFS66 Fourier transform infrared spectrometer at 2 cm^{-1} resolution in the double-sided/forward−backward acquisition mode. A liquid nitrogen-cooled midband MCT detector was used. Fourier transformation of the interferogram was performed with the Blackman-Harris-3-term apodization function, the Mertz phase correction mode, and a zero filling factor of 4. A total of 256 interferograms were accumulated and coadded. The absorption spectra were obtained from the ratio of the single channel intensity spectra of the sample to the single channel intensity spectra of the corresponding buffer reference at the respective temperatures.

The infrared absorption spectra were baseline corrected by fitting the left and the right sides of the spectrum, where no CO stretch band appears, using a cubic polynomial function. The baseline-corrected spectra were then fitted with Gaussians using a selfmade software package as previously described (*28*). The spectrum of the arginine-bound complexes consisted of only a single slightly asymmetric band that was fitted with the logarithmic normal distribution function (*28*) to get parameters describing the spectrum quantitatively.

Flashphotolysis Studies. The flashphotolysis system used has been described earlier (*32*, *33*). Flashphotolysis of the CO ligand was induced at 25 K by the frequency doubled output at 532 nm of a Q-switched Nd:YAG laser (Surelite I from Continuum). Before the sample was illuminated for 2 min (2 mJ/pulse, 10 Hz repetition rate), it was cooled to 25 K in the dark. Absorbance infrared difference spectra [$\Delta A(\nu)$] between the photodissociated and the CO-bound protein were obtained from the ratio of the single channel intensity spectra after (I_{light}) and before (I_{dark}) the illumination and by subsequent calculation of the negative logarithm $\Delta A(\nu) = -\log(I_{light}/I_{dark})$. Five hundred scans were accumulated for each intensity spectrum. The CO stretch vibration bands of the bound CO ligand appeared as negative signals, while the CO stretch bands of the photodissociated CO molecules corresponded to the positive signals in the infrared difference spectra.

RESULTS

Figure 1 shows the experimental infrared spectra for the iron CO ligand which have not been baseline-corrected. For better comparison, the spectra were normalized to the same peak area because the iNOSox concentration was not exactly the same in all samples. In the absence of arginine, the spectra showed a broad band with the maximum between 1945 and 1950 cm^{-1}.The addition of arginine shifted the band

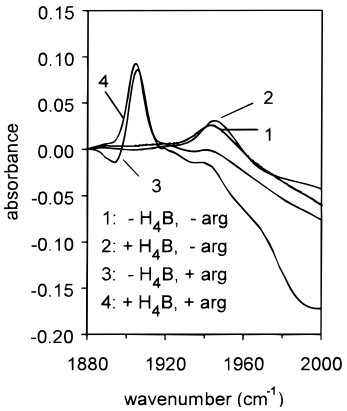

FIGURE 1: Experimental infrared spectra of iNOSox at 273 K in the absence or in the presence of either tetrahydrobiopterin (H_4B) and/or L-arginine (arg), without baseline correction. Spectra are normalized to the same area under the peak in the range of 1920−1980 cm^{-1} and in the range of 1890−1920 cm^{-1} for arginine-free iNOSox and arginine-bound iNOSox, respectively. 100 μm spacer; 17.8 mM EPPS, pH 7.6, 5.5−5.95 mM DTT, 57.7% (v/v) glycerol, 1.14 mM H_4B, 20−21 mM arginine; concentration of iNOSox: 0.5−1 mM; detailed conditions see Materials and Methods.

to a low frequency at about 1905 cm^{-1}. A very small band between 1940 and 1955 cm^{-1} was still detected in the arginine complexes but showed no temperature effect. It is possible that remaining arginine-free iNOSox or residual P420, which is a denatured form of iNOSox, could have caused this small band. However, the arginine concentration of 20−21 mM was high enough for complete binding of arginine even to the highly concentrated iNOSox (0.5−1 mM) [The arginine dissociation constant is in the micromolar range (*30*, *34*)]. Also P420 was unlikely to be the reason for this small band. Some P420 was present in the sample in the absence of H_4B as indicated by the shoulder around 420 nm on the characteristic Soret band (insets in Figure 2A and Figure 4A), however no P420 was seen for the H_4B-bound sample (insets in Figure 3A and Figure 4B). In both cases, however, we saw the small band between 1940 and 1955 cm^{-1} in the infrared spectrum of the arginine complex. Therefore, we conclude that it is a baseline artifact and will not further consider this band to investigate.

Characteristic band conversions and shifts of the real CO stretch mode bands are observed when the temperature is changed. In the following section, the temperature effect will be demonstrated using the baseline-corrected spectra.

iNOSox in the Absence of Arginine. Figure 2A shows the CO-stretch mode infrared spectrum of iNOSox in the absence of H_4B and arginine in the EPPS/DTT buffer system for selected temperatures between 20 and 298 K. At 298 K, a single broad CO stretch mode spectrum is observed at about 1945 cm^{-1}. For temperatures lower than 200 K, two major subconformers are clearly visible and are characterized by CO stretch frequencies at about 1954−1955 cm^{-1} and at about 1944−1945 cm^{-1}. Fitting the spectra with different line shapes including Gauss, Lorentz, Voigt, and logarithmic normal distribution (*28*) revealed that the spectra are more complex. The simplest model that fits the spectra with three Gaussians is shown in Figure 2B (Table 1). At 25 K, the frequencies of these bands are about 1935, 1943, and 1954 cm^{-1}. The first two bands will be regarded as a subband ensemble E1. The third band is very broad (width ~22 cm^{-1}), which indicates that this band is actually also an ensemble

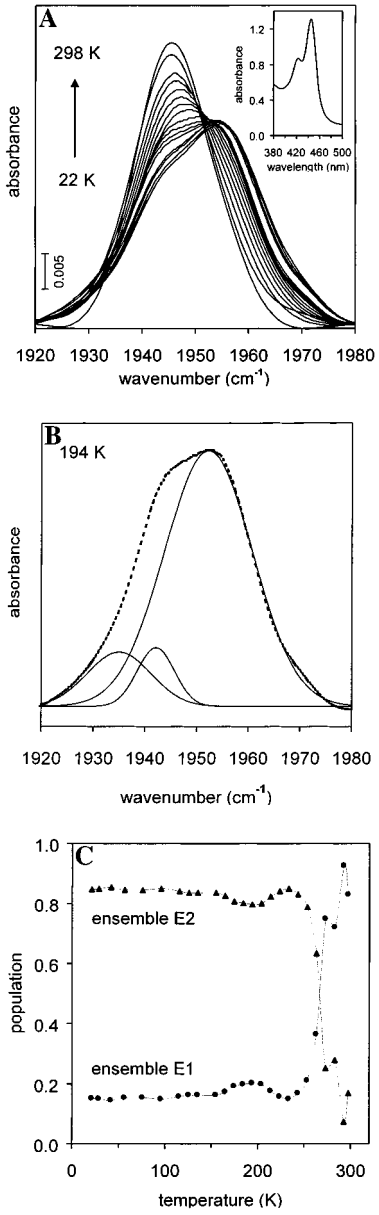

FIGURE 2: CO-stretch mode infrared spectrum of iNOSox in the absence of H_4B and arginine, 17.8 mM EPPS buffer, pH 7.6, 5.5 mM DTT, 57.7% (v/v) glycerol; (A) for selected temperatures between 20 and 298 K, area-normalized spectra; inset: UV−vis spectrum (Soret band) of the infrared sample directly measured in the infrared cell before the infrared study; (B) decomposition of the CO stretch mode infrared spectrum with three Gaussians (minimum fit model) for 194 K as an example; (C) population of the two major subband ensembles E1 (at 1930 and 1945 cm^{-1}) and E2 (at 1955 cm^{-1}) as a function of the temperature.

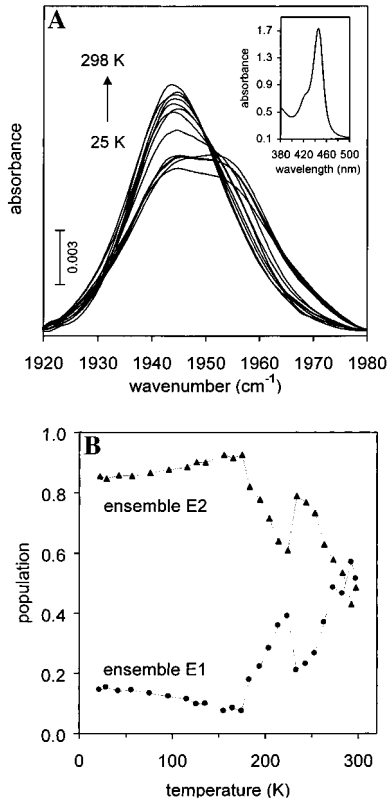

FIGURE 3: CO-stretch mode infrared spectrum of iNOSox in the absence of arginine and in the presence of H_4B, 17.8 mM EPPS buffer, pH 7.6, 1.1 mM H_4B, 5.94 mM DTT, and 57.7% (v/v) glycerol; (A) for selected temperatures between 20 and 298 K, area-normalized spectra; inset: UV−vis spectrum (Soret band) of the infrared sample directly measured in the infrared cell before the infrared study; (B) population of the two major subband ensembles E1 (at 1930 and 1943 cm^{-1}) and E2 (at 1951 cm^{-1}) as a function of the temperature.

of several bands of subconformers with slightly disordered heme environments (ensemble E2). Figure 2C demonstrates that population exchange between both major subband ensembles takes place only above 220−230 K. Using a mixture of potassium phosphate buffer and glycerol as solvent instead of the EPPS−glycerol buffer system, the CO stretch modes behave qualitatively similar (Table 1, spectra not shown). Addition of H_4B to iNOSox does not qualitatively change the spectrum (Figure 3A) as well as the temperature behavior of the CO ligand stretch mode spectral parameters (Figure 3B).

iNOSox in the Presence of Arginine. The addition of arginine to iNOSox in the absence of H_4B has a significant effect on the CO stretch mode spectrum. A sharp single band with a width of smaller than 10 cm^{-1} and a very low CO stretch frequency of 1905 cm^{-1} was observed at 292 K for iNOSox in the EPPS/DTT/glycerol buffer (Figure 4A, Table 1). These values are only slightly changed in the phosphate buffer/glycerol mixture (1905.6 cm^{-1}, Table 1). However, the exchange of H_2O by D_2O led to a shift of the band by ~0.8 to 1904.8 cm^{-1} accompanied by a small broadening (Figure 4B). Addition of H_4B shifts the band from 1905 to 1904.6 cm^{-1} (Figure 4C).

Cooling the samples to 25 K induced a sharpening and a shift of the band to lower frequencies (Table 1). The most striking temperature effect, however, was the almost linear downshift of the band in the temperature range between 250 and 25 K (Figure 5A). In all three cases, the CO stretch band of the arginine-bound iNOSox could not be fitted with a pure Gaussian. The optimal fit was obtained with the logarithmic normal distribution function (*28*) revealing an asymmetry factor slightly larger than 1. This indicated the asymmetry to be at the higher frequency side of the absorption band (Table 1). The width of the band is constant at temperatures lower than 100 K but showed a systematic increase when the temperature is elevated (Figure 5B). In the case of the sample without H_4B, an additional break in the relation between the width and the temperature was observed between 200 and 250 K due to a phase transition.

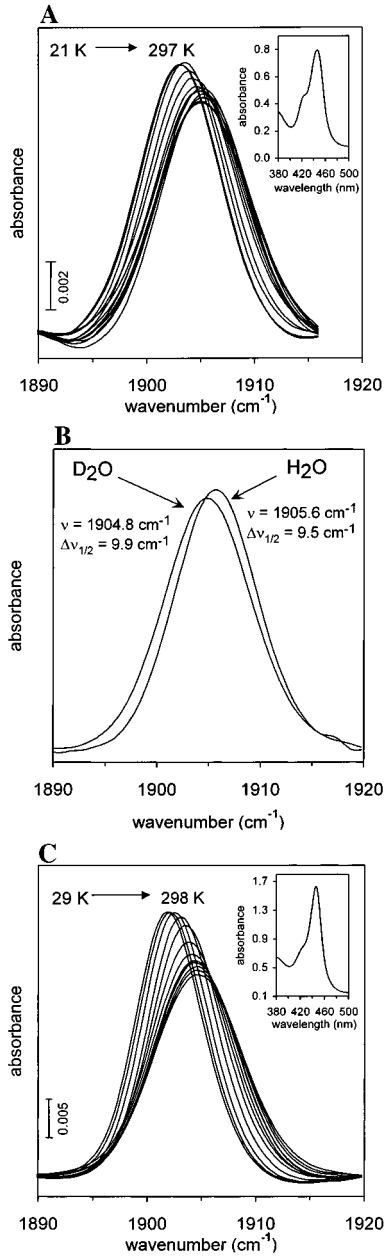

FIGURE 4: CO-stretch mode infrared spectrum of iNOSox in the presence of arginine; (A) in the absence of H_4B, selected temperatures between 20 and 298 K, area-normalized spectra; 17.8 mM EPPS buffer, pH 7.6, 5.5 mM DTT, 57.7% (v/v) glycerol, and 21 mM arginine; inset: UV−vis spectrum (Soret band) of the infrared sample directly measured in the infrared cell before the infrared study; (B) in the absence of H_4B, H_2O/D_2O exchange, 50 mM potassium phosphate buffer, pH 7, 50% glycerol, and 21 mM arginine, 295 K; (C) in the presence of H_4B, selected temperatures between 20 and 298 K, area-normalized spectra; 17.8 mM EPPS buffer, pH 7.6, 1.14 mM H_4B, 5.94 mM DTT, 57.7% (v/v) glycerol, and 22 mM arginine; inset: UV−vis spectrum (Soret band) of the infrared sample directly measured in the infrared cell before the infrared study.

CO Flashphotolysis. The active site of iNOSox was further characterized by CO flashphotolysis at 25 K. At this low temperature, the photodissociated CO ligand cannot leave the heme pocket. The CO stretch mode of the CO ligand in the photodissociated state (B state) appeared as a positive band in the infrared difference spectrum to the iron-bound CO ligand spectrum (A state, negative band). In the case of negligible CO rebinding, the negative A state bands should reflect the subband ensembles E1 and E2 as discussed above. The intensity of the B state bands was weaker by a factor of approximately 11−23 as compared to the A state bands, and they appeared in the region between 2118 and 2150 cm^{-1}. For iNOSox, in the absence of arginine and H_4B, the two major A states were seen as negative, strongly overlapping bands (Figure 6A). Curve fitting revealed two major bands at 1954.7 and 1944 cm^{-1} with one minor band at about 1935 cm^{-1} (Table 2) corresponding to E2 and E1, respectively. In the B state spectral region, a broad and asymmetric band appeared that was also an overlap of two major bands and one minor bands. For the sample in potassium phosphate buffer/glycerol, the two major subbands were better resolved. In the presence of H_4B, arginine-free iNOSox showed also at least two major A state subbands (corresponding to the ensembles E1 and E2) with an additional contribution of a shoulder at about 1914 cm^{-1} (Figure 6A). The B state band is very broad. However, the fit was not unequivocal; therefore, only the apparent CO stretch mode frequencies are given in Table 2.

In the presence of arginine, weak sidebands at 1922 and 1936 cm^{-1} are seen beside the major band at 1905 cm^{-1} (Figure 6B). These weak sidebands are difficult to resolve in the dark spectra because of baseline problems that do not exist in the flashphotolysis difference spectra.

DISCUSSION

The results of the present infrared studies on the iNOS oxygenase domain furnish three important points that are discussed below:

(i) Arginine-free iNOSox Exhibits Two Subconformer Ensembles. In the absence of arginine, the CO stretch mode reflects multiple subconformations that may be classified in two major substate ensembles. Ensemble E1 is characterized by CO stretch mode frequencies between 1930 and 1945 cm^{-1}, and ensemble E2 has a mean frequency at about 1955 cm^{-1}. Changes in temperature induce an interconversion between both substate ensembles. The population of ensemble E2 is favored at lower temperatures. The most significant population change is observed for the temperature range above the glass transition temperature at about 180 K. Below this temperature, the population ratio is almost constant. However, the CO stretch mode reflects also the complicated processes taking place when the protein−solvent mixture passes the phase transition between 250 and 180 K. A similar behavior has also been observed for cytochrome $P450_{cam}$ (*28*, *31*) and various other proteins (*35*, *36*).

The nature of the buffer system does not qualitatively change this behavior although the ratio of the population of both ensembles is quantitatively different. In the EPPS buffer system, the ensemble E2 was favored already at room temperature while in potassium phosphate buffer both ensembles were present in equal proportion. We excluded the possibility that the residual P420 seen in the H_4B-free sample (inset in Figure 2A) contributed significantly to the temperature-induced interconversion of the two major bands because the same subband interconversion behavior was also observed for the H_4B-bound protein which revealed no P420 at all (inset in Figure 3A).

Two subconformers, as discussed above, were also observed recently using resonance Raman measurements on

Table 1: CO Stretch Vibration Modes of INOSox Obtained by Curve Fitting of the Experimental Infrared Spectra

	292 K			25 K		
protein[a]	ν(CO) (cm^{-1})	$\Delta\nu_{1/2}$ (cm^{-1})	population	ν(CO) (cm^{-1})	$\Delta\nu_{1/2}$ (cm^{-1})	population
no arginine						
no H_4B, KP	1929.3 ± 0.5	11.2 ± 0.7	0.05	1937.6 ± 1.6	14.2 ± 1.5	0.15
	1943.4 ± 0.8	16.1 ± 1.0	0.55	1943.2 ± 0.1	8.3 ± 0.3	0.20
	1954.2 ± 1.2	16.8 ± 0.9	0.40	1956.4 ± 0.1	19.3 ± 0.2	0.65
no H_4B, EPPS	1935.4 ± 9.4	22.1 ± 8.0	0.10	1935.3 ± 2.6	14.8 ± 2.8	0.09
	1945.6 ± 0.1	15.9 ± 0.5	0.83	1942.1 ± 0.3	8.9 ± 1.0	0.07
	1956.8 ± 0.2	10.2 ± 0.3	0.07	1954.2 ± 0.1	21.4 ± 0.2	0.84
plus H_4B, EPPS	1929.8 ± 0.7	8.2 ± 2.4	0.00[c]	1934.0 ± 1.4	13.7 ± 1.0	0.09
	1942.9 ± 0.1	16.5 ± 0.4	0.56	1941.5 ± 0.3	8.9 ± 0.8	0.06
	1950.6 ± 1.8	24.8 ± 1.7	0.43	1950.9 ± 0.2	25.0 ± 0.3	0.85
protein[a]	ν(CO) (cm^{-1})	$\Delta\nu_{1/2}$ (cm^{-1})	asymmetry[b]	ν(CO) (cm^{-1})	$\Delta\nu_{1/2}$ (cm^{-1})	asymmetry[b]
plus arginine						
no H_4B, KP	1905.63 ± 0.02	9.51 ± 0.03	1.04	1904.85 ± 0.02	8.90 ± 0.04	1.12
no H_4B, EPPS	1905.04 ± 0.02	9.98 ± 0.04	1.07	1903.06 ± 0.01	8.79 ± 0.03	0.99
plus H_4B, EPPS	1904.60 ± 0.01	9.54 ± 0.02	1.05	1901.91 ± 0.03	7.38 ± 0.05	1.06

[a] Gauss fit for samples without arginine, logarithmic normal distribution fit for samples with arginine; KP, potassium phosphate buffer/glycerol mixture; EPPS, EPPS/glycerol mixture. [b] Asymmetry factor in logarithmic normal distribution function (*28*). [c] Smaller than 0.001.

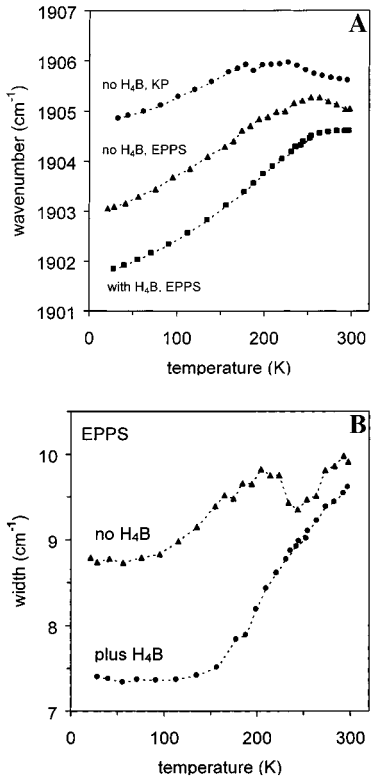

FIGURE 5: CO stretch mode parameters of iNOSox in the presence of arginine as a function of the temperature; (A) frequency, 50 mM potassium phosphate buffer, pH 7, 50% glycerol, 21 mM arginine (KP) and 17.8 mM EPPS buffer, pH 7.6, without or with 1.14 mM H_4B, 5.94 mM DTT, 57.7% (v/v) glycerol, and 22 mM arginine (EPPS); (B) width (fit with the logarithmic normal distribution).

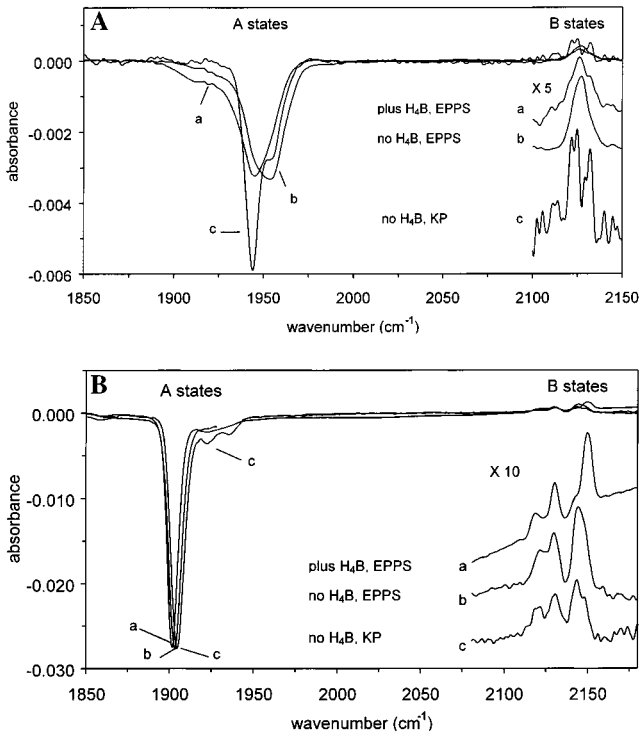

FIGURE 6: CO flashphotolysis infrared difference spectra (CO dissociated minus CO bound) at 25 K; (A) iNOSox in the absence of arginine: (a) with 1.1 mM H_4B, 17.8 mM EPPS buffer, pH 7.6, 5.94 mM DTT, and 57.7% (v/v) glycerol; (b) without H_4B, 17.8 mM EPPS buffer, pH 7.6, 5.5 mM DTT, and 57.7% (v/v) glycerol; (c) without H_4B in 50 mM phosphate buffer, pH 7.07, and 50% (v/v) glycerol; (B) iNOSox in the presence of arginine: (a) with 1.14 mM H_4B, 5.94 mM DTT, 57.7% (v/v) glycerol, and 22 mM arginine; (b) without H_4B, 17.8 mM EPPS buffer, pH 7.6, 5.5 mM DTT, 57.7% (v/v) glycerol, and 21 mM arginine; (c) without H_4B in 50 mM phosphate buffer, pH 7.07, and 50% (v/v) glycerol.

nNOS (*37*). These subconformers were characterized by stretch mode frequencies of the Fe−C bond and the C−O bond at 502 and 1930 cm^{-1} (α-form) and at about 486 and 1949 cm^{-1} (β-form), respectively. The α- and the β-forms may correspond to the subconformation ensembles E1 and E2, respectively, observed in our study. The α-form has been assigned to a "closed" conformation, while the β-form should represent an "open" conformation. This interpretation seems to be in agreement with our conclusion from extensive studies on cytochrome $P450_{cam}$ bound with various substrates (*29*) and indicates a critical role of water molecules for CO stretch modes at higher frequencies and for the population equilibrium of the subconformational states.

The binding of tetrahydrobiopterin does not change qualitatively this interpretation. The subband ensembles E1 and E2 are still present but show slightly changed population ratios and temperature effects. This may be explained by

Table 2: CO Stretch Vibration Modes of INOSox Observed in CO Flashphotolysis Infrared Difference Spectra at 25 K

protein	ν(CO) (cm^{-1})[a] A states	B states	area ratio[b]
no arginine			
no H_4B, KP	1944.1	2131.9	11[d]
	1953.6	2123.4	
no H_4B, EPPS	1935.4[f]	2133.6[f]	19
	1944.0	2127.8	
	1954.7	2123.2	
plus H_4B, EPPS	1945.6[c]	2126.0	18
plus arginine			
no H_4B, KP	1905.4	2145.0	23
	1922.0[f]	2131.0	
	1936.0[f]	2120.0	
no H_4B, EPPS	1903.5	2144.5	16[e]
	nd	2130.0	
	nd	2120.4	
plus H_4B, EPPS	1901.8	2150.2	21
	1922.3[f]	2130.7	
		2118.7	

[a] Decomposition by Gaussians using BRUKER IR (OPUS) software. [b] Ratio of the total area of A state bands to the total area of B state bands. [c] Apparent CO stretch mode frequencies without curve fitting. [d] Supposed to be too small because of noisy B state spectrum. [e] Supposed to be too small because of baseline artifact in A state spectrum. [f] Minor bands; nd, not detected because of baseline artifact; KP, potassium phosphate buffer/glycerol mixture; EPPS, EPPS/glycerol mixture

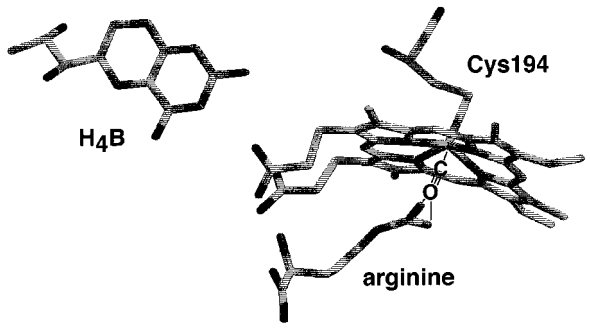

FIGURE 7: Structure of the heme pocket of iNOS indicating the binding sites of tetrahydrobiopterin (H_4B) and arginine. The CO ligand binding site and the possible interaction mode with arginine are sketched and are not part of the crystal structure. Coordinates are taken from PDB entry code 1NOD (13).

small structural changes due to hydrogen bonding of H_4B to the propionate of the heme (Figure 7) (*13*, *15*, *16*) resulting in changed disorder of water molecules in the heme pocket. Indeed, water molecules on the distal side of the heme have been found in the crystal structure of iNOSox in the presence of H_4B (*13*). The recently observed effect of H_4B on the selective protection of N-terminal hairpin hook proteolysis and its swapping interaction across the subunit (*30*, *38*, *39*) may not necessarily affect the local heme environment and may therefore not be reflected in the CO stretch infrared spectrum. This function of H_4B in protecting some parts of the protein may also explain the influence on the CO binding rate that is reflected in two different phases with a larger contribution of the slow rate versus the fast one as described earlier (*40*, *41*). This effect on the dynamics of the structure should not be reflected in the population equilibrium of the subconformers.

(ii) Arginine Binding Induces the Formation of a Hydrogen Bond to the Iron-Bound CO Ligand. Arginine binding shifts the CO stretch mode frequency to a very low value around 1905 cm^{-1}. Such a low frequency has also been observed for horseradish peroxidase at low pH (*42*−*44*) and was assigned to originate from the hydrogen bond of a distal amino acid residue to the CO ligand. A similar situation like in horseradish peroxidase may be induced by arginine binding to iNOSox. The sensitivity of the CO stretch mode against H_2O/D_2O exchange would also be in line with this conclusion. However, the downshift by ∼0.8 cm^{-1} is rather small compared to horseradish peroxidase for which a shift by ∼2.5 cm^{-1} has been observed (*45*). The hydrogen bond might rather be formed between the guanidinium group of arginine than between an amino acid side group and the CO ligand. Indeed, the recently published crystal structure of the iNOS dimer in the presence of arginine strongly supports this conclusion (*13*). The terminal nitrogens of the arginine guanidinium group are positioned ∼4 Å from the heme iron (Figure 7). This would be consistent with an usual hydrogen bonding distance between the terminal oxygen atom of the CO ligand and the arginine nitrogen of approximately 2.7−2.9 Å. The systematic decrease of the CO stretch mode frequency with decreasing temperature down to 20 K is the most striking observation. Usually, frequency shifts are found during cooling to the glass transition temperature of around 180−200 K, while at lower temperatures the frequencies are nearly constant (*28*, *31*). This is also the case for iNOSox in the absence of arginine (data not shown). The strong temperature-dependent shift of the CO stretch mode in the arginine complex, however, would be in line with the conclusion that a hydrogen bond to the CO ligand exists. Recently, Demmel et al. (*46*) demonstrated that the amide I band (peptide CO stretch mode) of myoglobin has stretch modes that are shifted to lower frequencies with lowering the temperature, if the vibrating group is involved in hydrogen bonding. Volume contraction during cooling is the physical origin that is accompanied by the strengthening of hydrogen bonds (*47*). Frauenfelder et al. (*48*) have shown that the myoglobin protein contracts by 3% of the total volume when its crystal is cooled from 300 to 80 K. The contraction might not be isotropic, if one considers the protein interior. This may result in a stronger or lesser extent of bond shortening of hydrogen bonds in specific parts of the protein. Assuming a strong hydrogen bond to the CO ligand and a rigid active site protein structure in the iNOSox−arginine complex, the volume contraction could lead to a shortening of the distance between CO and the arginine guanidinium nitrogen atom involved in the hydrogen bond and therefore to a decrease of the CO stretch mode frequency.

The thermal volume expansion coefficient α can be estimated from the frequency shift by eq 1 (46).

$$\alpha = -\gamma/\nu(\mathrm{CO})\,[\partial\nu(\mathrm{CO})/\partial \mathrm{T}] \qquad (1)$$

γ is a parameter characterizing the particular system (Grüneisen parameter) and has a value of approximately 1 in most cases. Assuming the value of 1 for iNOSox and taking the mean value of the CO stretch mode frequencies in the considered temperature range for ν(CO), the following expansion coefficients have been estimated: $2.9 \times 10^{-6}\ K^{-1}$ [iNOSox in phosphate buffer; range 140−180 K, mean ν(CO) = 1905.69 cm^{-1}]; $5.8 \times 10^{-6}\ K^{-1}$ [iNOSox in EPPS buffer, range 140−220 K, mean ν(CO) = 1904.55 cm^{-1}],

and 7.6×10^{-6} K^{-1} [iNOSox in the presence of H_4B, EPPS buffer, range 150−240 K, mean ν(CO) = 1903.43 cm^{-1}]. From this rough estimate, we may conclude that the active site structure is more rigid or coupled with the protein environment when H_4B is bound. So, the structural stress induced by the protein expansion/contraction is better mediated to the CO ligand.

In principle, one has to consider a strengthening of the hydrogen bond network around the negatively charged cystein iron ligand on the proximal heme side in NOS when the protein structure contracts with decreasing temperature. This would however lower the negative net charge and diminish the charge donation ability of the cystein ligand to the CO ligand coordinated to the heme iron in the trans position. A lower charge donation would result in an increase of the CO stretch mode frequency with cooling, this is however not observed.

More detailed experimental and theoretical studies are however required to verify our assignment of a hydrogen bond between arginine and the CO ligand. Unfortunately, a pH dependence study will not help to clarify the point because the pK_a of the arginine guanidinium group is too high (>12) thereby excluding any studies without denaturation of the protein. Use of arginine analogues, which do not bear a group that can donate a hydrogen bond to the CO ligand, is an alternative approach and is now under investigation.

(iii) The Photodissociated CO Ligand has Several Docking Sites in the Heme Pocket. Arginine Binding May Modulate the Charge on the Proximal Cysteinate Ligand. At low temperatures (<180 K), the photodissociated CO molecule cannot leave the heme pocket because the required protein motions for its exit are damped or frozen (*49*). However, CO can however rebind to the iron from the protein matrix and heme pocket (geminate rebinding), which has also been observed for NOS (*40*, *50*). At very low temperatures (<30 K) also the migration of the photodissociated CO in the protein matrix is prevented, and the CO will stay at specific docking sites (so-called B states). The stretch vibration of this docked CO ligand is an additional sensitive probe for the heme pocket. It appears in the region between 2118 and 2150 cm^{-1}. Studies on various substrate complexes of cytochrome $P450_{cam}$ indicated that a low stretch mode frequency of the iron-bound CO ligand (A state) may be related to a high B state CO stretch mode frequency (*27*). For iNOSox, we see a similar relation although the relative intensities of the A state subbands do not match those of the B state subbands. Nevertheless, when we assign the B state band with the highest stretch mode frequency to the A state band with the lowest frequency then we get a straight line (Figure 8, Table 2). Following the same assignment for myoglobin mutants and the wild type reported by Braunstein et al. (*51*), we find roughly a similar correlation but with a shifted line. Such a relation might indicate that the CO molecule has the same heme environment in the iron-bound as well as in the photodissociated form and thereby suggesting that the CO ligand stays near the heme. Indeed for myoglobin, the crystal structure shows that the CO ligand stays near the iron, almost parallel to the heme plane after photodissociation (*52*). Concerning the position of the straight line, the A/B state correlation seems to reflect a similar situation like the correlation between the C−O/Fe−CO stretch mode frequencies observed for many heme proteins (*25*, *37*, *53*). In these correlations, the different lines observed for hemoglobins and P450 have been explained by the different proximal ligand. The line for P450 is shifted along the axis of the A state CO stretch frequency to lower values because of the negative charge at the proximal cysteinate ligand (*53*). Keeping this in mind, it is interesting to note that iNOSox in the absence and in the presence of arginine follow different lines. One may suggest from Figure 8 that in the presence of arginine the charge at the proximal cysteinate ligand is more negative than in the absence of arginine. Therefore, arginine does not only induce a hydrogen bond to the CO ligand on the distal side but might also affect the hydrogen bond network around the proximal iron-bound cystein ligand observed in the crystal structure (*12*). It is likely mediated indirectly by conformational changes.

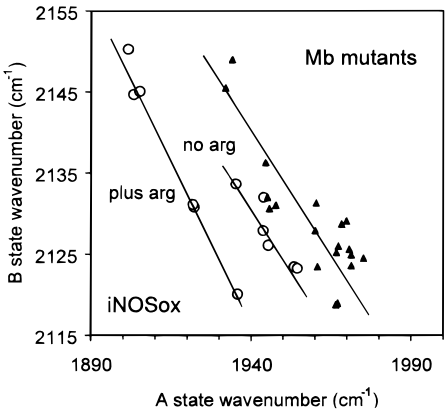

FIGURE 8: Relation between CO stretch mode frequencies of the iron-bound (A state) and the photodissociated (B state) CO molecule of iNOSox (open circles) (see Table 2) in comparison to myoglobin mutants (solid triangles) [data from Braunstein et al. (51)].

CONCLUSION

The most interesting result of the present infrared studies is the indication that in the arginine-bound iNOSox the iron-bound CO ligand is hydrogen bonded to a hydrogen donor. The hydrogen donor is very likely the arginine substrate itself. It is reasonable to transfer this conclusion to the physiologically relevant dioxygen complex, which implies that one intermediate step in the NOS reaction cycle is the proton donation from the substrate arginine to the iron-bound dioxygen complex to facilitate the O−O bond cleavage. However, the recent resonance Raman study of the dioxygen complex (*22*) seems to be in contradiction. These studies revealed that the ν(O−O) stretch vibration frequency of the O_2-complex obtained by rapid mixing is insensitive to the presence of the substrate and of the biopterin and shows a value of 1135 cm^{-1}. This observation is somewhat surprising since resonance Raman studies of the CO and the NO complexes of ferrous NOS clearly indicate an influence of the substrate binding on the iron-ligand and/or ligand stretch modes (*37*, *54*). For example, the ν(Fe−NO) appears at 536 and 549 cm^{-1} in the absence and in the presence of arginine, respectively (*54*). According to the rule given by Feltham and Enemark (*55*), ferrous NO complexes have a bent Fe−N−O geometry and are similar to the O_2 complexes. In particular, these resonance Raman studies on the ferrous NO complex exclude Fe−O−O bending as a reason for the different substrate effects on the ligand stretch modes of the

CO and the O_2 complexes as suggested by Couture et al. (*22*). So, whether the suggested hydrogen bond is also relevant for the dioxygen complex and whether it may be implicated in the oxygen activation remains still an open issue and has to be studied in more detail.

ACKNOWLEDGMENT

We are grateful to Udo Heinemann for carefully reading the manuscript and for critical comments. Brian Crane is acknowledged for helpful discussions.

REFERENCES

1. MacMicking, J., Xie, Q. W., and Nathan, C. (1997) *Annu. Rev. Immunol. 15*, 323−350.
2. Michel, T., and Feron, O. (1997) *J. Clin. Invest. 100*, 2146−2152.
3. Kröncke, K.-D., Fehsel, K., and Kolb-Bachofen, V. (1997) *Nitric Oxide 1*, 107−120.
4. Griffith, O. W., and Stuehr, D. J. (1995) *Annu. Rev. Physiol. 57*, 707−736.
5. Knowles, R. G., and Moncada, S. (1994) *Biochem. J. 298*, 249−258.
6. Masters, B. S. S., McMillan, K., Sheta, K., Nishimura, E. A., Roman, L. J., and Martásek, P. (1996) *FASEB J. 10*, 552−558.
7. Stuehr, D. J. (1999*) Biochim. Biophys. Acta 1411*, 217−230.
8. Xie, Q.-w., Cho, H. J., Calaycay, J., Mumford, R. A., Swiderek, K. M., Lee, T. D., Ding, A., Troso, T., and Nathan, C. (1992) *Science 256*, 225−228.
9. Ghosh, D. K., and Stuehr, D. J. (1995) *Biochemistry 34*, 801−807.
10. Sheta, E. A., McMillan, K., and Masters, B. S. S. (1994) *J. Biol. Chem. 269*, 15147−15153.
11. Sessa, W. C., Harrison, J. K., Barber, C. M., Zeng, D., Durieux, M., D'Angelo, D. D., Lynch, K. R., and Peach, M. J. (1992) *J. Biol. Chem. 267*, 15274−15276.
12. Crane, B. R., Arvai, A. S., Gachhui, R., Wu, C., Ghosh, D. K., Getzoff, E. D., Stuehr, D. J., and Tainer, J. A. (1997) *Science 278*, 425−431.
13. Crane, B. R., Arvai, A. S., Ghosh, D. K., Wu, C., Getzoff, E. D., Stuehr, D. J., and Tainer, J. A. (1998) *Sciences 279*, 2121−2126.
14. Crane, B. R., Rosenfeld, R. J., Arvai, A. S., Ghosh, D. K., Ghosh, S., Tainer, J. A., Stuehr, D. J., and Getzoff, E. D. (1999) *EMBO J. 18*, 6271−6281.
15. Raman, C. S., Li, H., Martásek, P., Král, V., Masters, B. S., and Poulos, T. L. (1998) *Cell 95*, 939−950.
16. Fischmann, T. O., Hruza, A., Da Niu, X., Fossetta, J. D., Lunn, C. A., Dolphin, E., Prongay, A. J., Reichert, P., Lundell, D. J., Narula, S. K., and Weber, P. C. (1999) *Nat. Struct. Biol. 6*, 233−242.
17. Li, H., Raman, C. S., Glaser, C. B., Blasko, E., Young, T. A., Parkinson, J. F., Whitlow, M., and Poulos, T. L. (1999) *J. Biol. Chem. 274*, 21276−21284.
18. White, K. A., and Marletta, M. A. (1992) *Biochemistry 31*, 6627−6631.
19. Abu-Soud, H. M., Gachhui, R., Raushel, F., and Stuehr, D. J. (1997) *J. Biol. Chem. 272*, 17349−17353.
20. Bec, N., Gorren, A. C. F., Voelker, C., Mayer, B., and Lange, R. (1998) *J. Biol. Chem. 273*, 13502−13508.
21. Ledbetter, A. P., McMillan, K., Roman, L. J., Masters, B. S. S., Dawson, J. H., and Sono, M. (1999) *Biochemistry 38*, 8014−8021.
22. Couture, M., Stuehr, D. J., and Rousseau, D. L. (2000) *J. Biol. Chem. 275*, 3201−3205.
23. Cupp-Vickery, J. R., Han, O., Hutchinson, C. R., and Poulos, T. L. (1996) *Nat. Struct. Biol. 3*, 632−637.
24. Vidakovic, M., Sligar, S. G., Li, H., and Poulos, T. L. (1998) *Biochemistry 37*, 9211−9219.
25. Li, X.-Y., and Spiro, T. G. (1988) *J. Am. Chem. Soc. 110*, 6024−6033.
26. Jung, C., Hui Bon Hoa, G., Schröder, K.-L., Simon, M., and Doucet, J. P. (1992) *Biochemistry 31*, 12855−12862.
27. Jung, C., Scholl, R., Frauenfelder, H., and Hui Bon Hoa, G. (1992) in *Cytochrome P-450: Biochemistry and Biophysics* (Archakov, A. I., and Bachmanova, G. I., Eds.) pp 33−38, INCO-TNC Joint Stock Company, Moscow.
28. Jung, C., Ristau, O., Schulze, H., and Sligar, S. G. (1996) *Eur. J. Biochem. 235*, 660−669.
29. Jung, C., Schulze, H., and Deprez, E. (1996) *Biochemistry 35*, 15088−15094.
30. Ghosh, D. K., Wu, C., Pitters, E., Moloney, M., Werner, E. R., Mayer, B., and Stuehr, D. J. (1997) *Biochemistry 36*, 10609−10619.
31. Schulze, H., Ristau, O., and Jung, C. (1994) *Eur. J. Biochem. 224*, 1047−1055.
32. Contzen, J., and Jung, C. (1998) *Biochemistry 37*, 4317−4324.
33. Contzen, J., and Jung, C. (1999) *Biochemistry 38*, 16253−16260.
34. Gachhui, R., Ghosh, D. K., Wu, C., Parkinson, J., Crane, B. R., and Stuehr, D. J. (1997) *Biochemistry 36*, 5097−5103.
35. Doster, W., Bachleitner, A., Dunau, R., Hiebl, M., and Lüscher, E. (1986) *Biophys. J. 50*, 213−219.
36. Mayer, E. (1994) *J. Am. Chem. Soc. 116*, 10571−10577.
37. Wang, J., Stuehr, D. J., and Rousseau, D. L. (1997) *Biochemistry 36*, 4595−4606.
38. Ghosh, D. K., Crane, B. R., Ghosh, S., Wolan, D., Gachhui, R., Crooks, R., Presta, A., Tainer, J. A., Getzoff, E. D., and Stuehr, D. J. (1999) *EMBO J. 18*, 6260−6271.
39. Ghosh, S., Wolan, D., Adak, S., Crane, B. R., Kwon, N. S., Tainer, J. A., Getzoff, E. D., and Stuehr, D. J. (1999) *J. Biol. Chem. 274*, 24100−24112.
40. Scheele, J. S., Kharitonov, V. G., Martásek, P., Roman, L. J., Sharma, V. S., Masters, B. S. S., and Magde, D. (1997) *J. Biol. Chem. 272*, 12523−12528.
41. Abu-Soud, H. M., Wu, C., Ghosh, D. K., and Stuehr, D. J. (1998) *Biochemistry 37*, 3777−3786.
42. Barlow, C. H., Ohlsson, P.-I., and Paul, K.-G. (1976) *Biochemistry 15*, 2225−2229.
43. Evangelista-Kirkup, R., Smulevich, G., and Spiro, T. C. (1986) *Biochemistry 25*, 4420−4425.
44. Uno, T., Nishimura, Y., Tsuboi, M., Makino, R., Iizuka, T., and Ishimura, Y. (1987) *J. Biol. Chem. 262*, 4549−4556.
45. Smith, M. L., Ohlsson, P.-I., and Paul, K. G. (1983) *FEBS Lett. 163*, 303−305.
46. Demmel, F., Doster, W., Petry, W., and Schulte, A. (1997) *Eur. Biophys. J. 26*, 327−335.
47. Kaposi, A. D., Fidy, J., Manas, E. S., Vanderkooi, J. M., and Wright, W. W. (1999) *Biochim. Biophys. Acta 1435*, 41−50.
48. Frauenfelder, H., Hartman, H., Karplus, M., Kuntz, I. D., Kuriyan, J., Parak, F., Petsko, G. A., Ringe, D., Tilton, R. F., Connolly, M., and Max, N. (1987) *Biochemistry 26*, 254−261.
49. Frauenfelder, H. (1997) in *Physics of Biological Systems - From Molecules to Species* (Flyvbjerg, H., Hertz, J., Jensem, M. H., Mouritsen, O. G., and Sneppen, K., Eds.) pp 29−60, Springer-Verlag, Berlin, Heidelberg.
50. Tetreau, C., Tourbez, M., Gorren, A., Mayer, B., and Lavalette, D. (1999) *Biochemistry 38*, 7210−7218.
51. Braunstein, D. P., Chu, K., Egeberg, K. D., Frauenfelder, H., Mourant, J. R., Nienhaus, U., Ormos, P., Sligar, S. G., Springer, B. A., and Young, R. D. (1993) *Biophys. J. 65*, 2447−2454.
52. Schlichting, I., Berendzen, J., Phillips, G. N., Jr., and Sweet, R. M. (1994) *Nature 371*, 808−812.
53. Legrand, N., Bondon, A., Simonneaux, G., Jung, C., and Gill, E. (1995) *FEBS Lett. 364*, 152−156.
54. Wang, J., Rousseau, D. L., Abu-Soud, H. M., and Stuehr, D. J. (1994) *Proc. Natl. Acad. Sci. U.S.A.* 91, 10512−10516.
55. Feltham, R. D., and Enemark, J. H. (1981) *Top. Stereochem. 12*, 155−215.

BI0003792